Relationships between PEMFC Cathode Kinetic Losses and Contaminants' Dipole Moment and Adsorption Energy on Pt

Jean St-Pierre,[*,z] Yunfeng Zhai,[*] and Junjie Ge[a]

Hawaii Natural Energy Institute, School of Ocean and Earth Science and Technology, University of Hawaii - Manoa, Honolulu, Hawaii 96822, USA

A database summarizing the effects of 21 contaminants on the performance of proton exchange membrane fuel cells (PEMFCs) was used to examine relationships between cathode kinetic losses and contaminant physicochemical parameters. Impedance spectroscopy data were employed to obtain oxygen reduction kinetic resistances by fitting data in the 10−158 Hz range to a simplified equivalent circuit. The contaminant dipole moment and the adsorption energy of the contaminant on a Pt surface were chosen as parameters. Dipole moments did not correlate with dimensionless cathode kinetic resistances. In contrast, adsorption energies were quantitatively and linearly correlated with minimum dimensionless cathode kinetic resistances. Contaminants influence the oxygen reduction for contaminant adsorption energies smaller than −24.5 kJ mol^{-1}, a value near the high limit of the adsorption energy of O_2 on Pt. Dimensionless cathode kinetic resistances linearly increase with decreasing O_2 adsorption energies below −24.5 kJ mol^{-1}. Measured total cell voltage losses are mostly larger than the cathode kinetic losses calculated from kinetic resistance changes, which indicates the existence of other sources of performance degradation. Modifications to the experimental procedure are proposed to ensure that data are comparable on a similar basis and improve the correlation between contaminant adsorption energy and kinetic cell voltage losses.

Manuscript submitted October 27, 2015; revised manuscript received December 26, 2015. Published January 5, 2016. This was Paper 1528 presented at the Phoenix, Arizona Meeting of the Society, October 11−15, 2015.

PEMFCs are attractive energy conversion devices. However, improvements are still required to meet the strict demands of automotive and other markets. PEMFCs are expected to be durable but are exposed to a variety of contaminants either present in air and hydrogen or released by fuel cell system materials, which may be deleterious to performance.[1–3] Only a small fraction of the large number of likely contaminants have been investigated. For example, only 21 ambient air species from a list of more than 200 candidates were recently studied.[4] Furthermore, fuel cell contamination tests require significant resources and may last several tens or a few hundreds of hours, even if accelerated conditions achieved with higher contaminant concentrations are used. As a result, there is a need to develop a simpler method to predict the impact of contaminants on fuel cell performance.

A prediction method for the performance loss associated with contamination has not been suggested for PEMFCs. However, the use of a molecule dipole moment was proposed to correlate the half-wave potential of the oxygen reduction reaction.[5] Only 5 contaminants were considered, and data were obtained with a thin film catalyst layer electrode mounted in a conventional three-electrode cell filled with an aqueous electrolyte maintained at room temperature. These operating conditions are significantly different from the PEMFC environment with a solid electrolyte and the presence of a gas diffusion layer covering the catalyst layer.

The PEMFC performance database resulting from separate tests performed with 21 airborne contaminants[4] is reexamined with the purpose of exploring the usefulness of two correlations between the kinetic loss at steady state and a contaminant physicochemical parameter. The contaminant dipole moment is first considered, thus significantly extending the range of the previous study[5] from 5 to 21 species. Data are also correlated with the contaminant adsorption energy on Pt. These efforts draw their inspiration from work in the catalysis field with the use of linear relationships between adsorption energies of similar chemical species to increase the efficiency of catalyst performance predictions, simplify descriptions of catalyst surface reactivity, etc.[6] Present results clarify the information necessary to establish more reliable and predictive correlations for PEMFC degradation.

Experimental

The PEMFC design, operating conditions and impedance spectroscopy diagnostics were previously documented and are only summarized here. Additional details are available in the cited literature.[4,7–9]

A custom-made single cell with a 50 cm^2 active area was employed. Triple- and double-channel serpentine flow fields were used for the cathode and anode, respectively. The membrane/electrode assembly was composed of SGL 25 BC gas diffusion layers and a Gore catalyst coated membrane (0.4/0.4 mg Pt cm^{-2}, 50% Pt/C, 18 μm thick membrane). A new membrane/electrode assembly was used for each contamination test, and the observed variability in kinetic resistance is representative of the catalyst-coated membrane manufacturing process (mean/standard deviation are 0.189/0.058 and 0.137/0.047 Ω cm^{-2} for wet and dry reactant streams, respectively). The average cell voltage of all membrane/electrode assemblies before contamination was characterized by a 10 and a 4 mV standard deviation for wet and dry reactant streams, respectively. The cell was operated with the following conditions: 45°C, 1 A cm^{-2}, air with 20 ppm contaminant/H_2 (with the exception of bisphenol A (0.1 ppm), bromomethane (50 ppm), butane (100 ppm) and ozone (95/83 ppm) for wet/dry conditions), 2/2 stoichiometry, 50/100 or 0/0 (humidifiers are bypassed) % relative humidity, 10/10 kPag back pressure at the cell outlet. A 45°C temperature was selected as a compromise to simultaneously maximize kinetic and ohmic losses with the objective of facilitating contaminant down selection. The contaminant was injected into the reactant stream after the humidifier to avoid losses by dissolution in water. During contaminant injection, the humidifier temperature was raised to maintain the relative humidity constant of the air. For most tests, gas cylinders filled with air/contaminant mixtures were used. However, for ozone, a generator was utilized whereas a temperature-controlled holder was employed to sublimate naphthalene and 2,2-bis(4-hydroxyphenyl)propane.

Impedance spectra were acquired from 0.1 to 10 kHz using a Solartron SI1260 instrument and Stanford Research SR560 low-noise preamplifiers. The ZPlot and ZView (Scribner Associates) software

*Electrochemical Society Active Member.
[a]Present address: Changchun Institute of Applied Chemistry, Chinese Academy of Sciences, Changchun, Jilin 130022, People's Republic of China.
[z]E-mail: jsp7@hawaii.edu

packages were used to control tests/acquire data and fit an equivalent circuit model to experimental data, respectively. An alternating current perturbation with a 0.75 A amplitude, resulting in a cell voltage change of approximately 5 mV, was applied to the cell at a direct current of 50 A.

Results and Discussion

Analysis approach.—In a previous report, a method was proposed to select airborne contaminants from a list of more than 200 candidates to study their effects on a PEMFC.[4] In the first step, the number of contaminants was reduced to 21 candidates by using several qualitative criteria (1st tier species). In the second step, all 21 1st tier species were tested using operating conditions summarized in the experimental section. The contaminant candidates were further reduced to a shorter list of 7 candidates (2nd tier species) using 2 quantitative criteria. Second tier species were the subject of detailed studies to determine contamination mechanisms. Only the 1st tier species dataset is used in this report to correlate PEMFC performance losses to contaminant physicochemical parameters (Table I). The database contains cell voltage transients and impedance spectra acquired before, during and after a temporary contamination period. The use of impedance spectroscopy during the galvanostatic experiments was more economical because only a single experiment was needed to assess the different cell performance losses, and diagnostics could be completed without affecting the transient test sequence (baseline, contamination phase, recovery phase), operating conditions and the catalyst surface state (reactant and contaminant species, adsorbates' coverage, etc.). By comparison, polarization curves would have required additional experiments with other current densities and oxidant gas compositions to separate kinetic, ohmic and mass transfer contributions. Furthermore, associated changes in current density/cathode potential during the acquisition of polarization curves would modify the catalyst surface state. This conclusion equally applies to the use of cyclic voltammetry for the estimation of the coverage of contaminant adsorbates.

The analysis focuses on kinetic cell performance losses because Pt is a common catalyst used for many processes.[46] Therefore, it was expected that a larger amount of information would be available for physicochemical parameters characterizing interactions between Pt and 1st tier species. In contrast, significantly less information is available for the interactions between the ion exchange polymer, either ionomer (catalyst layers component) or membrane, and 1st tier species (ohmic performance losses).[47–50] With regard to mass transfer performance losses, their cause in the presence of contaminants is not yet clear, and several possibilities exist including localized higher current densities (catalyst active area is reduced owing to contaminant adsorption, a situation equivalent to a catalyst loading decrease),[50–53] the potential dependence of contaminant adsorbates coverage leading to an additional capacitive or inductive loop in the frequency range usually ascribed to mass transfer[54–57] and contaminant adsorption on C (liquid water management).[58,59] Therefore, several physicochemical parameters may be necessary to correlate mass transfer performance losses.

Sample impedance spectra are depicted in Figures 1 and 2 for vinyl acetate and acetylene cases, respectively. Before contamination, the impedance loop observed in the ~10 to ~1000 Hz frequency range (Figures 1a and 2a) is ascribed to oxygen reduction (constant phase element CPE_c, kinetic resistance R_c). The faint shoulder at high frequencies (~1 to >1 kHz) is indicative of the small anode impact and the comparatively fast hydrogen oxidation reaction (capacitor C_a, kinetic resistance R_a). The low frequency loop (<10 Hz) is attributed to the slow transport of reactants/products and disappears at low current densities (generalized finite length Warburg element W_c). The remainder of the circuit elements are accounted by the membrane, conductors and contact resistances between components (resistance R), and cables (inductance L). The presence of vinyl acetate and acetylene in the airstream increases the diameter of both midrange and low frequency loops. Furthermore, a new process is present in the low frequency range with the appearance of an inductive behavior (positive imaginary impedance values). The new process is more prominent with acetylene (Figures 1c and 2c). An equivalent circuit model developed for SO_2 contamination[7] adequately represents impedance data (Figure 3a) for each contaminant in the PEMFC performance database before the contamination period.[4] However, the appearance of a new process invalidates the use of this equivalent circuit because it cannot reproduce the inductive behavior. Modifications have been suggested to consider this feature (Figures 3b and 3c) with the addition of either an R_1/C_1 parallel circuit[54,55] or an R_k/L_k series circuit.[56,57] A simpler equivalent circuit is used (Figure 3d) to extract the oxygen reduction resistance, the focus of the present study. This is necessary in part to keep the approach simple. Otherwise, the anticipated complexity associated with a multitude of contaminants that do not behave similarly would require the derivation of either several equivalent circuit models or many mathematical models based on physical phenomena to extract meaningful parameter values. Furthermore, a more detailed modeling approach would defeat the original purpose of developing a simple prediction method. Figures 1 and 2 show that the fitting process for the 10 to 158 Hz range ascribed to oxygen reduction in absence of contamination adequately reproduces the measured data even if the oxygen reduction characteristics have significantly changed as a result of contamination. For instance, the phase angle peak is shifted to lower frequencies (Figures 1c and 2c). Such changes in oxygen reduction reaction were noted before in the presence of contaminants (exchange current density, Tafel slope, H_2O_2 yield, etc).[5,60–65] It was impossible to obtain an oxygen reduction kinetic resistance value for naphthalene because the changes were too significant and the fitting algorithm led to an unreasonably large kinetic resistance value. Oxygen reduction kinetic resistances are listed in Table I and are correlated in the next 2 sections to the physicochemical parameters of the contaminants.

Dipole moment based correlation.—The dipole moment has previously been used to correlate the change in oxygen reduction reaction half-wave potential with the presence of contaminants in the aqueous liquid electrolyte.[5] It was proposed that the contaminant dipole moment would capture the essence of the electronic interactions between the organic contaminant and oxygen adsorbates bonded to the catalyst surface. It is emphasized that the half-wave potential reflects all performance losses, and the kinetic contribution was not isolated.

Dipole moments are listed in Table I. These are correlated to dimensionless kinetic resistances, the ratio of the kinetic resistance during the contamination period R_c to the kinetic resistance measured before the introduction of the contaminant R_{c0}, to minimize the variability observed between different membrane/electrode assemblies (R_{c0} and R_c values, Table I). Dimensionless kinetic resistances are plotted against dipole moments in Figure 4. A correlation was not found between these variables, an observation that contrasts with the previous report.[5] However, it is recognized that a linear correlation might be found for selected species. The data points of the 4 dry reactant streams that fall on the exemplary linear correlation line in Figure 4 (1,1-difluoroethane, acetonitrile, methyl tert-butyl ether, trichlorofluoromethane) has a correlation coefficient of 0.988. The absence of a correlation for the present larger dataset is attributed to the choice of the dipole moment, which characterizes only the contaminant molecules themselves and does not include surface effects such as adsorbate geometry and configuration on the catalyst surface. Therefore, a different and more appropriate contaminant physicochemical parameter was identified.

Adsorption energy based correlation.—The adsorption energy E_{ads} was selected as a more appropriate physicochemical parameter to represent the interactions between the contaminant and the catalyst surface because it includes not only electronic effects but also adsorbate geometries. From that standpoint, the adsorption energy is a more specific parameter and has recently been considered to correlate catalysis results.[6] However, published values do not constitute a uniform set (Table I) because most values were calculated whereas a few were also measured. In most cases, the Pt(111) crystal face, which is predominant in cubo-octahedral nano-sized particles,[66] was considered.

Table I. Contaminant dipole moment, adsorption parameters, and electrochemical stability parameters, oxygen reduction kinetic resistances, and cathode potentials during contamination.

		Kinetic resistance										
		50/100% relative humidity		0/0% relative humidity		Adsorption parameters		Electrochemical stability parameters			Cathode potential (V vs RHE)[i]	
Contaminant	Dipole moment (D)	Before contamination (Ω cm^2)	During contamination (Ω cm^2)	Before contamination (Ω cm^2)	During contamination (Ω cm^2)	Adsorption energy (kJ mol^{-1})	Catalyst surface and adsorbate configuration	Reduction (V vs RHE)	Oxidation (V vs RHE)	Electrode	50/100% relative humidity	0/0% relative humidity
1,1-difluoroethane[a]	2.671[10]	0.206	0.298	0.114	0.154							
1,1,1,2-tetrafluoroethane[b]	2.028[10]	0.201	0.229	0.118	0.134							
2,2-bis(4-hydroxyphenyl) propane[c]	1.41[11]	0.094	0.100	0.105	0.110							
Acetaldehyde	2.689[10]	0.248	0.214	0.110	0.088	−27[15]	Calculation with Pt(111) and atop $\eta^1\mu^1$(O) configuration[15]	<0.35 (0.09 peak)[31]	>0.6 (0.85 and 1.20 peaks),[31] >0.5 (0.7 peak) and 0.85[41]	Porous Pt,[31] Pt/C[41]	0.614	0.604
Acetone	2.88[12]			0.109	0.119	−39.6[16]	Calculation with Pt(111) and keto-isomer η^1(O) configuration[16]	No activity in 0−1.4 range[32]	No activity in 0−1.4 range[32]	Polycrystalline Pt[32]		0.688
Acetonitrile	3.92[10]	0.190	0.291	0.239	0.349							
Acetylene	0[10]	0.160	0.911	0.201	1.01	−50[17,18]	Measurement with Pt powder[17] Calculation with Pt(111) and three-fold site $\eta^2\eta^2$ configuration[18]	<0.23[33]	>0.65[42]	Pt,[33] porous Pt[42]	0.229	0.216
Bromomethane	1.811[10]	0.197	0.361	0.113	0.197	−59.8[19]	Measurement with Pt(111) single crystal[19]	−2.2[34] (C_2H_5Br, C_3H_7Br) <−1.4[35]	>1.6[35]	Pt and platinized Pt gauze[34]	0.407	0.405
Butane	0[10]	0.229	0.238			15.8[20,e], 12[21,e] 46.2 to 59.7[22,e]	Calculation with Pt(100) and with butane axis parallel to the surface[20] Measurement with Pt(111) single crystal[21] Measurement with Pt(111)[22]	Inert?	>0.24[43]	Pt black[43]	0.701	
Chlorobenzene	1.69[12]	0.191		0.114		−37.9[23,f], −116 to −130[24,f]	Calculation with Pt(001) and adsorption through the chlorine atom configuration[23] Calculation with Pt(111) and bridge(30) configuration (4 di-σ and 2 π-type interactions)[24]	<−2.20[36]	1.26 peak[44]	Hg,[36] Pt sheet[44]	0.144	0.151
Dichloromethane	1.601[10]	0.149	0.152									
Isopropanol	1.58[12]	0.227	0.224	0.114	0.118	−39.3[25]	Calculation with Pt(111) at 300 K[25]	<0.2[37]	>0.35 (0.70 and 1.30 peaks),[37] >0.32 (0.65 peak)[45]	Sputtered Pt,[37] Pt/C[45]	0.703	0.688
Methyl acetate	1.72[12]	0.237	0.234									
Methyl methacrylate	1.68[13]			0.207	0.422							
Methyl tert-butyl ether	1.25[14]	0.347	0.451	0.115	0.134							

Table I. (*Continued.*)

Contaminant	Dipole moment (D)	Kinetic resistance: 50/100% relative humidity, Before contamination (Ω cm^2)	Kinetic resistance: 50/100% relative humidity, During contamination (Ω cm^2)	Kinetic resistance: 0/0% relative humidity, Before contamination (Ω cm^2)	Kinetic resistance: 0/0% relative humidity, During contamination (Ω cm^2)	Adsorption parameters: Adsorption energy (kJ mol^{-1})	Adsorption parameters: Catalyst surface and adsorbate configuration	Electrochemical stability parameters: Reduction (V vs RHE)	Electrochemical stability parameters: Oxidation (V vs RHE)	Electrochemical stability parameters: Electrode	Cathode potential (V vs RHE)[i]: 50/100% relative humidity	Cathode potential (V vs RHE)[i]: 0/0% relative humidity
Naphthalene	0[13]	0.105	0.309	0.114	0.500	−126[26]	Calculation with Pt(111) and di-bridge[7] configuration[26]	<0-0.05[38]	1.35 peak with shoulders at 1 and 1.2[38]	Pt(111) and polycrystalline Pt[38]	0.203	0.195
Ozone	0.54[10]	0.102	0.103	0.111	0.099							
Propene	0.366[12]	0.19	0.296	0.236	0.338	−89.7[27,g] −72.2[28,g]	Calculation with Pt(111) and bridge di-σ configuration[27] Calculation with Pt(111) and di-σ configuration[28]	0.07 peak,[32] <0.2[39]	0.96 peak,[32] >0.6−1.6[39]	Polycrystalline Pt,[32] sputtered Pt[39]	0.515	0.480
Toluene	0.36[10]	0.178	0.495	0.117	0.187	−71[29,h] −75[30,h]	Calculation with Pt(111) and hollow site configuration[29] Measurement with Pt/C[30]	<0.1[40]	0.5−0.9 and 0.9−1.5[40]	Sputtered Pt[40]	0.242	0.231
Trichlorofluoromethane[d]	0.45[10]	0.168	0.169	0.122	0.131							
Vinyl acetate	1.781[10]	0.170	0.227	0.114	0.120							

[a]also referred to as HFC-152a.
[b]also referred to as HFC-134a.
[c]also referred to as bisphenol A.
[d]also referred to as CFC-11
[e]An average value of 13.9 kJ mol^{-1} is used for plotting and disregards the larger adsorption energy range.
[f]An average value of −123 kJ mol^{-1} is used for plotting, which assumes a bridge configuration at a low operating cathode potential.
[g]An average value of −81 kJ mol^{-1} is used for plotting.
[h]An average value of −73 kJ mol^{-1} is used for plotting.
[i]The average cathode potential before contamination is 0.714 (wet streams) and 0.707 (dry streams) V vs RHE.

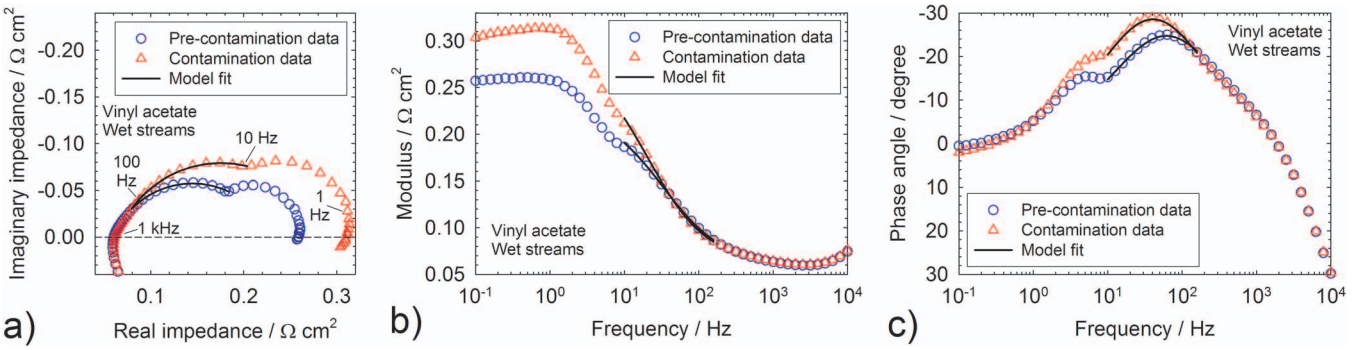

Figure 1. Impedance spectroscopy data obtained with a PEMFC before contamination and during contamination at steady state (symbols). Air + 20 ppm vinyl acetate/H_2, 50/100% relative humidity. A fit to the equivalent circuit model of Figure 3d for data in the 10 to 158 Hz range is indicated by a full line. a) Nyquist plot; b) Bode plot of impedance modulus, c) Bode plot of impedance phase angle.

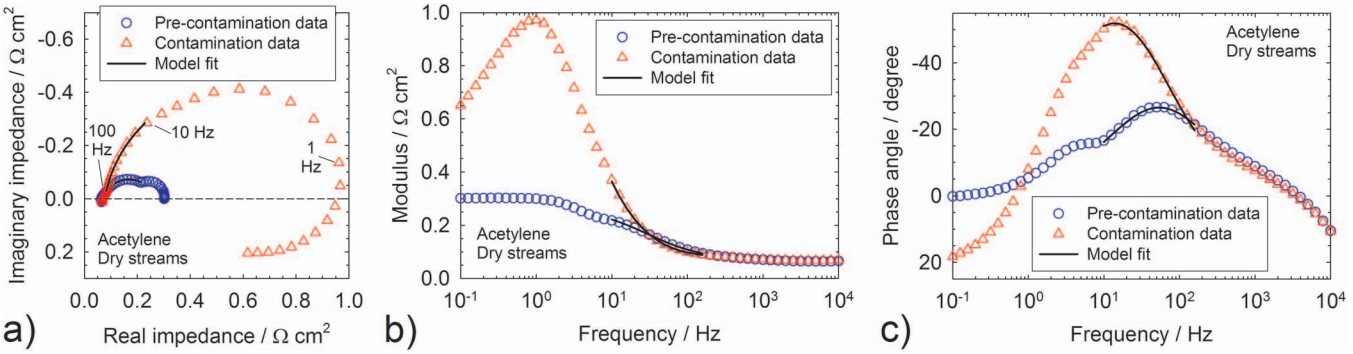

Figure 2. Impedance spectroscopy data obtained with a PEMFC before contamination and during contamination at steady state (symbols). Air + 20 ppm acetylene/H_2, 0/0% relative humidity. A fit to the equivalent circuit model of Figure 3d for data in the 10 to 158 Hz range is indicated by a full line. a) Nyquist plot; b) Bode plot of impedance modulus, c) Bode plot of impedance phase angle.

Two reports are focused on the Pt(100) crystal face and highlight the significant dependence of the adsorption energy on the exposed face (see chlorobenzene entries in Table I). Additionally, most adsorption energies were calculated and agree with measurements for acetylene and toluene (Table I). Calculations for propene and measurements for butane are also not necessarily consistent with significant differences between values (Table I).

The uniformity of the adsorption energy dataset highlights the necessity to examine the consistency of dimensionless kinetic resistances. Table II summarizes the parameters that affect the kinetic resistance and adsorption energy during contamination. Operating conditions,[30] the Pt surface configuration[66] and the fraction of Pt covered by the ionomer[67–69] (items 1, 2 and 4 in Table II) were either controlled or fixed by the membrane/electrode assembly choice. The butane and bromomethane concentrations were the only deviations from the controlled operating conditions (50 and 100 ppm, respectively, rather than 20 ppm for the other contaminants used for the adsorption energy correlation). However, even if the current density is constant, the cathode potential changes during the contamination period affect the outcome of adsorption and reactions. The cathode potential was maintained below the potential necessary for Pt oxidation (0.8 vs RHE).[70] The cell voltage before contamination was 0.658 V

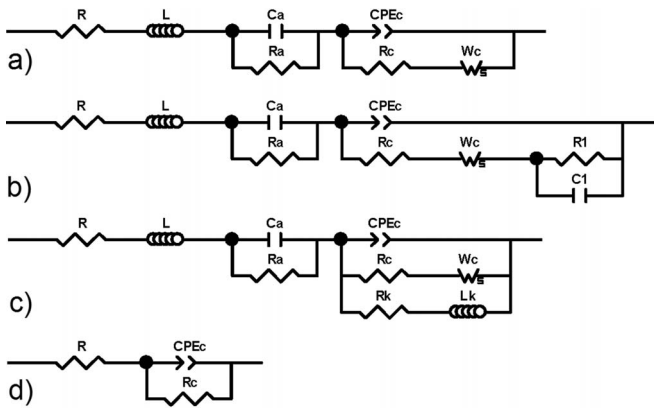

Figure 3. Equivalent circuit models for a PEMFC. a) Model for SO_2 contamination, b) Model for SO_2 contamination modified to capture inductive data (R_1/C_1 parallel circuit), c) Model for SO_2 contamination modified to capture inductive data (R_k/L_k series circuit), d) Simplified model for data attributed to O_2 reduction between 10 and 158 Hz.

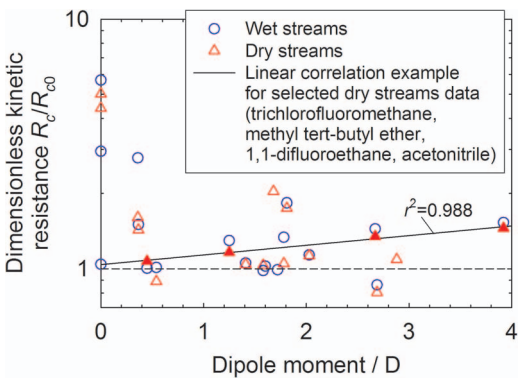

Figure 4. Dimensionless oxygen reduction kinetic resistances R_c/R_{c0} at steady state for 21 different contaminants as a function of the contaminant dipole moment and reactant stream humidity. Filled symbol data were used for the exemplary linear correlation.

Table II. Summary of the parameters associated with processes occurring during contamination.

PEMFC catalyst parameters of relevance to contamination
1. Operating conditions (contaminant partial pressure, temperature, etc.)
2. Pt surface configuration (crystal faces, edges, kinks, etc.)
3. Pt state (reduced, oxidized)
4. Phase in contact with the Pt surface (air, ionomer)
5. Adsorption isotherms for O_2, contaminant, and related species including activation energy and adsorbate interactions and configurations (number of Pt sites occupied, mono- or multilayer adsorption, etc.)
6. Elementary chemical and electrochemical reactions and rate constants for O_2 reduction and contaminant oxidation or reduction

with wet streams and 0.646 V with dry streams. These values led to a cathode potential of 0.714 and 0.707 V vs RHE, respectively, with the assumption of an anode at 0 V vs RHE and a membrane/electrode assembly ohmic resistance of 0.056 and 0.061 Ω cm^2, respectively. Therefore, the Pt surface was in a reduced state for all cases (item 3, Table II). The contaminant adsorption energy on Pt is not the only relevant adsorption parameter of importance. Competitive adsorption with O_2 species, adsorbate configurations[15,25] and adsorbed layer thickness (mono- or multilayer) among others also play a role (item 5, Table II). These additional adsorption parameters affect the contaminant surface coverage even if the operating conditions and Pt surface are invariant and impact the development of a correlation because data are compared on a different basis. For instance, the adsorption energy is dependent on surface coverage.[30] The situation is further complicated by the possibility of chemical or electrochemical reactions that affect the surface coverage by adsorbates (item 6, Table II). Acetaldehyde, butane and isopropanol are electrochemically active at their corresponding cell operating potential (Table I). It is possible that adsorbate species are created that are either less or more strongly bound to the catalyst surface than the original contaminant.

Available adsorption energies on Pt are given in Table I. These are correlated to dimensionless kinetic resistances (Figure 5). Although some data points are scattered, two trends are observed for the lowest dimensionless kinetic resistances. For adsorption energies >-24.5 kJ mol^{-1}, contaminants have no effect on the oxygen reduction reaction (dimensionless kinetic resistance ~1, boundary A line, Figure 5). In contrast, for adsorption energies <-24.5 kJ mol^{-1}, contaminants have a negative effect on the oxygen reduction reaction, which progressively worsens for lower adsorption energies (dimensionless kinetic resistance >1, boundary B line, Figure 5). These observations are consistent with competitive adsorption between contaminant and O_2 species. The O_2 adsorption energy varies and depends on a number of factors including surface coverage, adsorption site and phase in contact with Pt (gas, ionomer).[71–73] An O_2 adsorption energy range was added to Figure 5. For contaminant adsorption energies >-24.5 kJ mol^{-1}, O_2 has a smaller adsorption energy and sticks more strongly to the catalyst surface than the contaminant. Therefore, the contaminant does not displace O_2 to a significant extent from the catalyst surface and does not have a significant effect on the kinetic resistance. However, for contaminant adsorption energies <-24.5 kJ mol^{-1}, competitive adsorption occurs and the contaminant partially displaces O_2 from the catalyst by blocking active sites, resulting in an increase in the dimensionless kinetic resistance. The adsorption energy of -24.5 kJ mol^{-1} separating boundary lines A and B is interpreted as an effective O_2 adsorption energy on Pt.

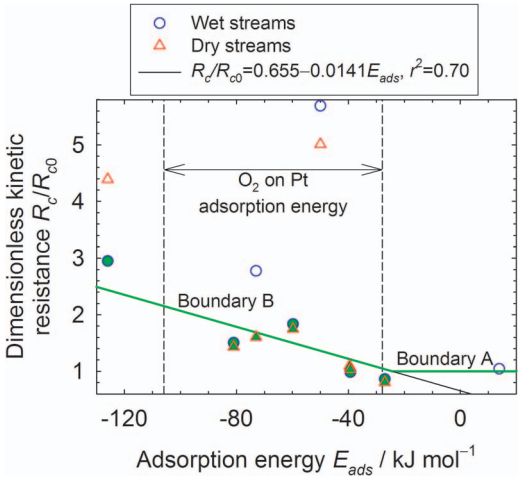

Figure 5. Dimensionless oxygen reduction kinetic resistances R_c/R_{c0} at steady state for 9 different contaminants as a function of the contaminant adsorption energy on Pt E_{ads} and reactant stream humidity. Boundaries A and B (Equation 1) lines indicate the absence of a contaminant effect and the minimum change in dimensionless kinetic resistance R_c/R_{c0}, respectively. Filled symbol data were used to determine the correlation of boundary B.

The boundary B line is described by (Figure 5)

$$\frac{R_c}{R_{c0}} = 0.655 - 0.0141 E_{ads} \text{ for } E_{ads} < -24.5 \text{ kJ mol}^{-1} \quad [1]$$

The relationship between the dimensionless kinetic resistance and the calculated kinetic cell voltage ΔV_c loss is given by

$$\Delta V_c = i\,(R_c - R_{c0}) \quad [2]$$

which makes use of the Figure 3d equivalent circuit to calculate the voltage drop across the kinetic resistance R_c. Rearrangement of Equation 2 leads to

$$\frac{R_c}{R_{c0}} = 1 + \frac{\Delta V_c}{i R_{c0}} \quad [3]$$

The best fit to Equation 3 yields a value of 0.169 Ω cm^2 for the average kinetic resistance before contamination (supplementary information Figure S1). More importantly, the combination of Equations 1 and 3 links the kinetic cell performance loss to the contaminant adsorption energy on Pt for operation at 1 A cm^{-2}, which could be used for predictive purposes with the limitations highlighted at the beginning of this section:

$$\Delta V_c = -R_{c0}\,(0.345 + 0.0141 E_{ads}) \text{ for } E_{ads} < -24.5 \text{ kJ mol}^{-1} \quad [4]$$

Kinetic resistances before contamination derived from impedance spectra are consistent with those calculated from Tafel plots. In Table I, kinetic resistances average to 0.189 Ω cm^2 for wet reactant streams. For Tafel behavior, the kinetic resistance is equal to the ratio of the Tafel slope and the current density (Equation 10.13 in Ref. 74) which leads, for example, to values of 0.137 and 0.151 Ω cm^2 at high current densities near 1 A cm^{-2} (supplementary information Figure S2). Additionally, a comparison between total cell voltage losses[4] and calculations for kinetic cell voltage losses (Figure 6) indicates that the use of Equation 2 is reasonable because most total values are either equal to or greater than kinetic values (Figure 6). In other words, other cell performance losses may be present during contamination in addition to kinetic losses. For instance, Figures 1 and 2 demonstrate that there is also an increase in the low frequency loop size (<10 Hz) during contamination, which is potentially due to either O_2 or H_2O mass transport changes or contaminant reactions. For the acetylene cases (Figure 2), the calculated kinetic loss is larger than the measured total loss and the pre-contamination steady-state cell voltage V_0. It is surmised that the large change in O_2 reduction kinetics that displaces the related phase angle peak from 50 to 15 Hz (Figure 2c) partially overlaps with the low frequency peak and introduces an error. This situation defines the limit of the impedance data analysis procedure.

Equation 4 represents a minimum value for the kinetic cell voltage loss because a few data points are located above boundary lines A

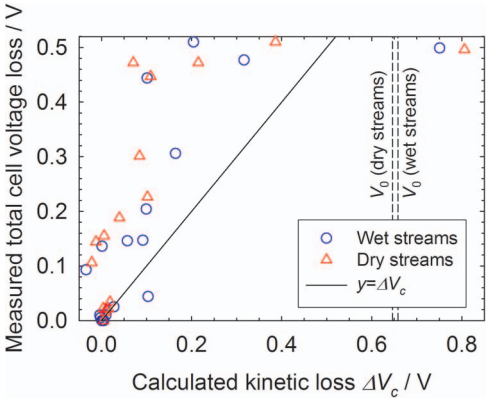

Figure 6. Measured total loss in cell voltage at steady state for a PEMFC exposed to 21 different contaminants ($V_a - V_b$ values from Table III of Reference 4) as a function of the calculated kinetic loss ΔV_c (Equation 2) and reactant stream humidity.

and B (Figure 5). Some of these data that pertain to acetylene ($E_{ads} = -50$ kJ mol^{-1}, Table I) and toluene ($E_{ads} = -73$ kJ mol^{-1}, Table I) indicate a larger dimensionless kinetic resistance for a larger reactant stream humidity. The addition of a water molecule to an alkene or alkyne is a common procedure to produce alcohols. It is possible that the alcohol product or an intermediate has larger adsorption energy on Pt than acetylene or toluene, thus accounting for the larger effect on the dimensionless kinetic resistance. However, such an explanation is not necessarily correct because reaction products in a fuel cell environment are not necessarily predictable. For instance, chlorobenzene reaction products detected in a fuel cell do not necessarily correspond to those resulting from a chemical surface reaction in the presence of adsorbed O_2 or an electrochemical reaction conducted in a liquid electrolyte without O_2.[9] This statement is partly confirmed by the observation that propene ($E_{ads} = -81$ kJ mol^{-1}, Table I) does not show a relative humidity effect, whereas naphthalene ($E_{ads} = -126$ kJ mol^{-1}, Table I) behaves differently with a larger change in dimensionless kinetic resistance for drier reactant streams (Figure 5).

Conclusions

A recently published database containing PEMFC performance losses due to a significant number of contaminants was reexamined with the objective of deriving a correlation based on a relevant contaminant physicochemical property. The adsorption energy yielded a correlation for the minimal kinetic performance loss. A modified experimental procedure is expected to provide a more precise correlation by ensuring that data are comparable on a similar basis. The contaminant adsorption energy on Pt should either be measured or calculated on a consistent basis for species of interest (same Pt face and surface coverage). The use of a uniform membrane/electrode assembly design and operating conditions was mentioned. However, a constant electrode potential rather than current density and a contaminant concentration adapted to specific contaminants are preferable to better control surface conditions (Pt state, electrochemical reaction rates) and maintain a constant contaminant, reaction intermediate or product surface coverage. The importance of the present analysis is emphasized in view of the large amount of resources that would be needed to improve Equation 1 based on these suggestions with the measurement of the adsorption energy on Pt and, the fuel cell performance for many contaminants and commercially relevant low Pt loading membrane/electrode assemblies.

Although inorganic contaminants were not considered in the present study, they are expected to behave in a similar manner as organic species because they may also adsorb on Pt. However, the mechanism of interaction between cations and the Pt surface is different from that for inorganic and organic contaminants. Therefore, the adsorption energy must be replaced by another more representative contaminant parameter to correlate cell performance losses and effects on the oxygen reduction reaction.[3,48,49,75–77] Furthermore, the isolation of the kinetic portion of the cell performance loss is experimentally difficult to achieve because cations simultaneously affect thermodynamic, kinetic, ohmic and mass transport losses.[48,49] As a result, models were used to obtain a better understanding of the relative contribution of each cell performance loss type.[78–82]

Acknowledgments

Authors are indebted to the United States Department of Energy for funding (award DE-EE0000467). The authors are grateful to the Hawaiian Electric Company for their ongoing support to the operations of the Hawaii Sustainable Energy Research Facility.

References

1. J. St-Pierre, in *Polymer Electrolyte Fuel Cell Durability*, F. N. Büchi, M. Inaba, and T. J. Schmidt, Editors, p. 289, Springer, New York (2009).
2. B. M. Besancon, V. Hasanov, R. Imbault-Lastapis, R. Benesch, M. Barrio, and M. J. Mølnvik, *Int. J. Hydrogen Energy*, **34**, 2350 (2009).
3. J. St-Pierre, M. Angelo, K. Bethune, J. Ge, S. Higgins, T. Reshetenko, M. Virji, and Y. Zhai, *Electrochem. Soc. Trans.*, **61**(23), 1 (2014).
4. J. St-Pierre, Y. Zhai, and M. S. Angelo, *J. Electrochem. Soc.*, **161**, F280 (2014); J. St-Pierre, Y. Zhai, and M. S. Angelo, *J. Electrochem. Soc.*,**162**, X7 (2015).
5. M. S. El-Deab, F. Kitamura, and T. Ohsaka, *J. Electrochem. Soc.*, **160**, F651 (2013).
6. M. M. Montemore and J. W. Medlin, *Catal. Sci. Technol.*, **4**, 3748 (2014).
7. Y. Zhai, G. Bender, K. Bethune, and R. Rocheleau, *J. Power Sources*, **247**, 40 (2014).
8. Y. Zhai and J. St-Pierre, *J. Power Sources*, **279**, 165 (2015).
9. Y. Zhai, O. Baturina, D. Ramaker, E. Farquhar, J. St-Pierre, and K. Swider-Lyons, *J. Phys. Chem. C*, **119**, 20328 (2015).
10. C. L. Yaws, *Thermophysical Properties of Chemicals and Hydrocarbons*, 2nd ed., Gulf Professional Publishing (2014).
11. A. I. Schäfer, L. D. Nghiem, and N. Oschmann, *J. Membr. Sci.*, **283**, 233 (2006).
12. *CRC Handbook of Chemistry and Physics*, 89th ed., D. R. Lide, Editor-in-chief, CRC Press, Boca Raton, FL (2008).
13. J. A. Dean, *Lange's Handbook of Chemistry*, 15th ed., McGraw-Hill (1999).
14. R. D. Suenram, F. J. Lovas, W. Pereyra, G. T. Fraser, and A. R. H. Walker, *J. Mol. Spectrosc.*, **181**, 67 (1997).
15. F. Delbecq and F. Vigné, *J. Phys. Chem. B*, **109**, 10797 (2005).
16. E. L. Jeffery, R. K. Mann, G. J. Hutchings, S. H. Taylor, and D. J. Willock, *Catal. Today*, **105**, 85 (2005).
17. T. Jacob and W. A. Goddard III, *J. Phys. Chem. B*, **109**, 297 (2005).
18. X. Lu, L. Liu, Y. Li, W. Guo, L. Zhao, and H. Shan, *Phys. Chem. Chem. Phys.*, **14**, 5642 (2012).
19. C. French and I. Harrison, *Surf. Sci.*, **387**, 11 (1997).
20. P. Légaré, P. S. Moussounda, and M. F. Haroun, *Surf. Sci.*, **600**, 2938 (2006).
21. I. Lee and F. Zaera, *J. Phys. Chem. C*, **111**, 10062 (2007).
22. K. Lee, Y. Morikawa, and D. C. Langreth, *Phys. Rev. B*, **82**, 155461 (2010).
23. T. Yoneda, T. Takido, and K. Konuma, *J. Mol. Catal. A*, **265**, 80 (2007).
24. V. Nieminen, K. Honkala, A. Taskinen, and D. Y. Murzin, *J. Phys. Chem. C*, **112**, 6822 (2008).
25. K. B. Tarmyshov and F. Müller-Plathe, *J. Chem. Phys.*, **126**, 074702 (2007).
26. G. Santarossa, M. Iannuzzi, A. Vargas, and A. Baiker, *Chem. Phys. Chem.*, **9**, 401 (2008).
27. M.-L. Yang, Y.-A. Zhu, C. Fan, Z.-J. Sui, D. Chen, and X.-G. Zhou, *J. Mol. Catal. A*, **321**, 42 (2010).
28. L. Nykänen and K. Honkala, *J. Phys. Chem. C*, **115**, 9578 (2011).
29. M. Saeys, M.-F. Reyniers, J. W. Thybaut, M. Neurock, and G. B. Marin, *J. Catal.*, **236**, 129 (2005).
30. W. G. Shim and S. C. Kim, *Appl. Surf. Sci.*, **256**, 5566 (2010).
31. J. Silva-Chong, E. Méndez, J. L. Rodríguez, M. C. Arévalo, and E. Pastor, *Electrochim. Acta*, **47**, 1441 (2002).
32. J. L. Stickney, M. P. Soriaga, A. T. Hubbard, and S. E. Anderson, *J. Electroanal. Chem.*, **125**, 73 (1981).
33. H. J. Davitt and L. F. Albright, *J. Electrochem. Soc.*, **118**, 236 (1971).
34. J. Simonet and D. G. Peters, *J. Electrochem. Soc.*, **151**, D7 (2004).
35. A. Tallec, *Électrochimie Organique - Synthèses et Mécanismes*, pp. 12 and 15, Masson, Paris (1985).
36. S. O. Farwell, F. A. Beland, and R. D. Geer, *Electroanal. Chem. Interf. Electrochem.*, **61**, 303 (1975).
37. E. Pastor, S. González, and A. J. Arvia, *J. Electroanal. Chem.*, **395**, 233 (1995).
38. T. Löffler, E. Drbalkova, P. Janderka, P. Königshoven, and H. Baltruschat, *J. Electroanal. Chem.*, **550–551**, 81 (2003).
39. M. Bełtowska-Brzezinska, T. Łuczak, H. Baltruschat, and U. Müller, *J. Phys. Chem. B*, **107**, 4793 (2003).
40. J. L. Rodríguez and E. Pastor, *Electrochim. Acta*, **45**, 4279 (2000).
41. H. Wang, Z. Jusys, and R. J. Behm, *Fuel Cells*, **4**, 113 (2004).
42. J. W. Johnson, H. Wroblowa, and J. O'M. Bockris, *J. Electrochem. Soc.*, **111**, 863 (1964).

43. J. A. Shropshire and H. H. Horowitz, *J. Electrochem. Soc.*, **113**, 490 (1966).
44. L. Liu, G. Zhao, M. Wu, Y. Lei, and R. Geng, *J. Hazard. Mater.*, **168**, 179 (2009).
45. C.-G. Lee, M. Umeda, and I. Uchida, *J. Power Sources*, **160**, 78 (2006).
46. B. C. Gates, *Chem. Rev.*, **95**, 511 (1995).
47. J. St-Pierre, *Electrochem. Soc. Trans.*, **41**(1), 307 (2011).
48. J. St-Pierre, *J. Power Sources*, **196**, 6274 (2011).
49. J. St-Pierre, *Int. J. Hydrogen Energy*, **36**, 5527 (2011).
50. J. St-Pierre, J. Ge, Y. Zhai, T. V. Reshetenko, and M. Angelo, *Electrochem. Soc. Trans.*, **58**(1), 519 (2013).
51. N. Nonoyama, S. Okazaki, A. Z. Weber, Y. Ikogi, and T. Yoshida, *J. Electrochem. Soc.*, **158**, B416 (2011).
52. T. A. Greszler, D. Caulk, and P. Sinha, *J. Electrochem. Soc.*, **159**, F831 (2012).
53. A. Z. Weber and A. Kusoglu, *J. Mater. Chem. A*, **2**, 17207 (2014).
54. R. E. Melnick and G. T. R. Palmore, *J. Phys. Chem. B*, **105**, 1012 (2001).
55. R. E. Melnick and G. T. R. Palmore, *J. Phys. Chem. B*, **105**, 9449 (2001).
56. X. Wang, I.-M. Hsing, Y.-J. Leng, and P.-L. Yue, *Electrochim. Acta*, **46**, 4397 (2001).
57. N. Wagner and E. Gülzow, *J. Power Sources*, **127**, 341 (2004).
58. L. Fournel, P. Mocho, J. L. Fanlo, and P. Le Cloirec, *Environ. Technol.*, **26**, 1277 (2005).
59. S. Giraudet, B. Boulinguiez, and P. Le Cloirec, *Energy Fuels*, **28**, 3924 (2014).
60. Y. Garsany, O. A. Baturina, and K. E. Swider-Lyons, *J. Electrochem. Soc.*, **154**, B670 (2007).
61. M. S. El-Deab, F. Kitamura, and T. Ohsaka, *J. Power Sources*, **229**, 65 (2013).
62. J. Ge, J. St-Pierre, and Y. Zhai, *Electrochim. Acta*, **133**, 65 (2014).
63. J. Ge, J. St-Pierre, and Y. Zhai, *Electrochim. Acta*, **134**, 272 (2014).
64. J. Ge, J. St-Pierre, and Y. Zhai, *Electrochim. Acta*, **138**, 437 (2014).
65. J. Ge, J. St-Pierre, and Y. Zhai, *Int. J. Hydrogen Energy*, **39**, 18351 (2014).
66. K. Kinoshita, *J. Electrochem. Soc.*, **137**, 845 (1990).
67. M. S. Wilson and S. Gottesfeld, *J. Appl. Electrochem.*, **22**, 1 (1992).
68. T. R. Ralph, G. A. Hards, N. J. Collis, J. E. Keating, S. A. Campbell, D. P. Wilkinson, M. Davis, J. St-Pierre, and M. C. Johnson, *J. Electrochem. Soc.*, **144**, 3845 (1997).
69. R. Subbaraman, D. Strmcnik, V. Stamenkovic, and N. M. Markovic, *J. Phys. Chem. C*, **114**, 8414 (2010).
70. M. Gattrell and B. MacDougall, in *Handbook of Fuel Cells – Fundamentals, Technology and Applications*, Vol. 2, W. Vielstich, H. A. Gasteiger, and A. Lam, Editors, p. 443, John Wiley and Sons (2003).
71. K. Matsuda and S. Harada, *Mater. Trans.*, **46**, 1058 (2005).
72. A. Ohma, T. Ichiya, K. Fushinobu, and K. Okazaki, *Surf. Sci.*, **604**, 965 (2010).
73. Z. Duan and G. Wang, *J. Phys. Chem. C*, **117**, 6284 (2013).
74. M. E. Orazem and B. Tribollet, *Electrochemical Impedance Spectroscopy*, p. 165, Wiley (2008).
75. D. Strmcnik, D. F. van der Vliet, K.-C. Chang, V. Komanicky, K. Kodama, H. You, V. R. Stamenkovic, and N. M. Marković, *J. Phys. Chem. Lett.*, **2**, 2733 (2011).
76. J. Durst, M. Chatenet, and F. Maillard, *Phys. Chem. Chem. Phys.*, **14**, 13000 (2012).
77. I. Katsounaros, W. B. Schneider, J. C. Meier, U. Benedikt, P. U. Biedermann, A. Cuesta, A. A. Auer, and K J. J. Mayrhofer, *Phys. Chem. Chem. Phys.*, **15**, 8058 (2013).
78. A. Z. Weber and C. Delacourt, *Fuel Cells*, **8**, 459 (2008).
79. B. L. Kienitz, H. Baskaran, and T. A. Zawodzinski Jr., *Electrochim. Acta*, **54**, 1671 (2009).
80. T. A. Greszler, T. E. Moylan, and H. A. Gasteiger, in *Handbook of Fuel Cells – Fundamentals, Technology and Applications*, Vol. 6, W. Vielstich, H. Yokokawa, and H. A. Gasteiger, Editors, p. 728, John Wiley, Chichester (2009).
81. M. F. Serincan, U. Pasaogullari, and T. Molter, *Int. J. Hydrogen Energy*, **35**, 5539 (2010).
82. M. A. Uddin and U. Pasaogullari, *J. Electrochem. Soc.*, **161**, F1081 (2014).